p-ISSN: 2301-6663, e-ISSN: 2477-250X
URL: http://ojs.ummetro.ac.id/index.php/turbo

Investigation of the Influence of Plate Thickness on Orifice Flow Using the Computational Fluid Dynamics Method

Mokhammad Bahtiar Rivai[1], James Julian[1*], Fitri Wahyuni[1], Riki Hendra Purba[1]

[1]Teknik Mesin, Universitas Pembangunan Nasional Veteran Jakarta
Jln. RS. Fatmawati Raya. Pd. Labu, Kec. Cilandak, Kota Depok, Jawa Barat 12450, Indonesia
**Corresponding author*: zames@upnvj.ac.id

Abstract

Piping systems provide effective fluid distribution and are crucial to industrial operations. Despite their effectiveness, flow control devices like orifice plates can result in significant pressure drop that can lower system efficiency and wear out the system's mechanical components. This study aims to optimize orifice plate design by examining the effect of plate thickness on flow characteristics using Computational Fluid Dynamics (CFD). Simulations were conducted on orifice plates with thicknesses ranging from 1.5T to 3.0T under Reynolds numbers from 10^4 to 10^6. Results show that increasing the thickness reduces pressure loss, with the 3T configuration achieving a 1.35% reduction compared to the baseline. Improvements are linked to a higher discharge coefficient (C_d), shorter flow reattachment distance (X_r), smaller recirculation zones, and reduced velocity through the orifice throat. These findings suggest that geometric modifications can enhance flow performance and reduce the risk of mechanical damage in piping systems.
Keywords**:** *CFD, orifice, piping, system, thickness*

1. Introduction

Piping systems are widely used across industries for efficient fluid transport, offering high capacity, low operational costs, and strong safety performance [1]. In the oil and gas sector, they are essential for supporting production and distribution processes [1, 2]. To improve efficiency, these systems often incorporate valves, filters, venturi tubes, bends, and orifice plates [3, 4]. Among these, orifice plates are the most commonly used due to their low maintenance, ease of installation, and simple design [4].

The concentric orifice plate, with a central hole, is popular for clean flow measurement due to its simplicity. Variants like eccentric, segmental, and quadrant-edge plates serve specific needs, such as handling bubbles, particles, and low Reynolds flows. Despite these benefits, orifice plates can cause adverse effects, including pressure drop and vibration [5]. For example, Cioncolini et al. found that increasing the thickness of the orifice plate can reduce the pressure drop [4]. Other studies have explored honeycomb-type orifice plates with modified thickness and geometry, showing reduced pressure and risk of cavitation and pipe deformation [6]. Research on multi-orifice plates with varying thicknesses has also shown more stable pressure behavior over a range of Reynolds numbers, improving flow control [7]. Additional research on orifice placement in pipe bends has shown the potential to prevent structural damage [8]. In contrast, studies on chamfered orifice plates have shown that pressure drop varies with chamfer angle, with specific angles improving flow characteristics [9].

Research has shown that using orifice plates in piping systems can significantly cause pressure drops. This phenomenon can negatively impact the stability of industrial production and distribution processes. Previous studies have indicated that to reduce the notable increase in pressure drop, adjusting the orifice plate from its ISO standard state is essential to ensure the piping system's efficiency. Additionally, existing literature has not thoroughly examined the effects of varying orifice plate thickness with a beta ratio of 0.6. Therefore, this study aims to investigate fluid flow characteristics as it passes through

DOI: http://dx.doi.org/10.24127/trb.v14i2.4286
Received June 14, 2025; Received in revised form December 26, 2025; Accepted December 28, 2025
Available online December 31 2025

an ISO standard orifice plate with a beta ratio of 0.6 and different thicknesses. Although many investigations have been into orifice plates, further research is needed to enhance current knowledge and address the adverse effects. The outcomes of this investigation are anticipated to furnish a foundational framework for future studies in this domain.

2. Methodology

2.1 Orifice Plate

As ISO 5167-2 specified, an orifice plate is a centrally positioned, perforated flow restriction device within a pipeline that induces a measurable pressure drop across its surfaces. This pressure drop, calculated from the difference between upstream and downstream pressures, is expressed using Equation 1. The D and D/2 pressure tapping method is widely adopted, positioning taps one diameter (D) upstream and half a diameter (D/2) downstream from the orifice plate by ISO 5167-2. Given that the orifice plate alters the measured mass flow rate, a discharge coefficient is applied to correct the flow calculation based on the observed pressure drop. As delineated by Equation 2, the discharge coefficient facilitates a more precise estimation of the actual flow rate [10, 11].

$$\Delta P = P_{upstream} - P_{downstream} \quad (1)$$

$$C_d = \frac{q_m \sqrt{1-\beta^4}}{\frac{\pi}{4} d^2 \sqrt{2\Delta P \rho}} \quad (2)$$

2.2 Geometries

This study analyzes fluid flow through an orifice plate within a two-dimensional incompressible system. The simulation geometry includes a long upstream pipe and a short downstream pipe with an orifice plate, designed to ensure fully developed flow before reaching the orifice and to maintain computational efficiency (Figure 1 and Table 1). The upstream length is determined using the entrance region length defined in Equation 3 [12, 13]. The orifice plate design follows ISO 5167-2, with thickness as the primary variable, while the orifice-to-pipe diameter ratio (β) is fixed at 0.6 due to its low standard deviation and stable pressure characteristics in turbulent flow [10]. The formula for β is provided in Equation 4.

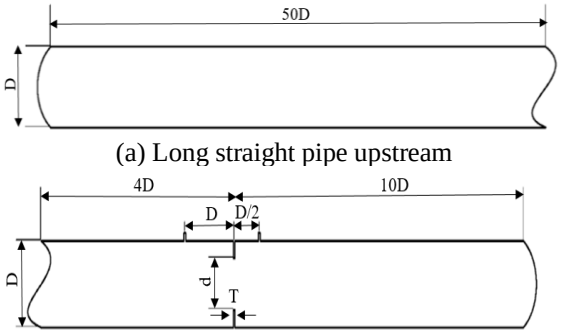

(a) Long straight pipe upstream

(b) Short straight pipe with an orifice plate

Figure 1. Detail geometries

Table 1. Parameter geometries

Parameter	Value (mm)
D	100.1
d	60.06
β	0.6
T_1 **(baseline)**	3.2
T_2	4.8
T_3	6.4
T_4	8
T_5	9.6

$$\frac{l_e}{D} = 4.4(Re)^{\frac{1}{6}} \quad (3)$$

$$\beta = \frac{d}{D} \quad (4)$$

2.3 Governing Equation

In this study, a Computational Fluid Dynamics (CFD) method using the Reynolds-Averaged Navier-Stokes (RANS) equation with continuity and momentum equations as shown in Equations 5 and 6 is used [14]. A realizable k-ε turbulence model improves simulations' accuracy in the turbulent regime. This model has proven superior to the standard k-ε model in capturing complex phenomena such as flow separation, recirculation, and pressure gradients. The model uses two transport equations: the turbulent kinetic energy (k) and the turbulent dissipation rate (ε); the

equation for k follows the standard model (Equation 7), while the equation for ε is modified to better account for eddy rms fluctuations, details of which are given in Equation 8 [15].

$$\frac{\partial \rho}{\partial t}+\frac{\partial(\rho u_i)}{\partial x_i}=0 \tag{5}$$

$$\frac{\partial}{\partial t}(\rho u_i)+\frac{\partial}{\partial x_i}(\rho u_i u_j)= -\frac{\partial \rho}{\partial x_i}+\frac{\partial}{\partial x_j}\left[\mu\left(\frac{\partial u_i}{\partial x_j}+\frac{\partial u_j}{\partial x_i}-\frac{2}{3}\delta_{ij}\frac{\partial u_i}{\partial x_i}\right)\right]+\frac{\partial}{\partial x_j}\left(-\rho\overline{u_i' u_j'}\right) \tag{6}$$

$$\frac{\partial}{\partial t}(\rho k)+\frac{\partial}{\partial x_i}(\rho k u_i)= \frac{\partial}{\partial x_j}\left[\left(\mu+\frac{\mu_t}{\sigma_k}\right)\frac{\partial k}{\partial x_j}\right]+G_k+G_b-\rho\varepsilon-Y_m \tag{7}$$

$$\frac{\partial}{\partial t}(\rho \varepsilon)+\frac{\partial}{\partial x_i}(\rho \varepsilon u_i)= \frac{\partial}{\partial x_j}\left[\left(\mu+\frac{\mu_t}{\sigma_\varepsilon}\right)\frac{\partial \varepsilon}{\partial x_j}\right]+\rho C_1 S\varepsilon -\rho C_2\frac{\varepsilon^2}{k+\sqrt{\vartheta\varepsilon}}+C_{1\varepsilon}\frac{\varepsilon}{k}C_{3\varepsilon}G_b+S_\varepsilon \tag{8}$$

2.4 Mesh and Boundary Conditions

A structured mesh composed of quadrilateral elements was used in this study. Two-dimensional geometrical models were constructed, each featuring a long upstream pipe and a short downstream pipe surrounding the orifice plate. Both configurations assumed symmetry to simplify the flow domain. Boundary conditions were applied to ensure fully developed flow at the inlet by specifying inlet velocity, applying no-slip conditions on all solid walls, and setting zero gauge pressure at the outlet. The downstream pipe inlet conditions—velocity magnitude, turbulent kinetic energy (TKE), and dissipation rate (ε)—were derived from the results of the upstream pipe simulation [16]. The orifice plate and all wall surfaces were treated as no-slip boundaries. Fluid velocity was determined based on the Reynolds number range specified by ISO 5167-2 ($10^4 \leq Re \leq 10^6$), as shown in Equation 9. Mesh configuration and boundary condition details are presented in Figure 2.

$$Re=\frac{\rho D V}{\mu} \tag{9}$$

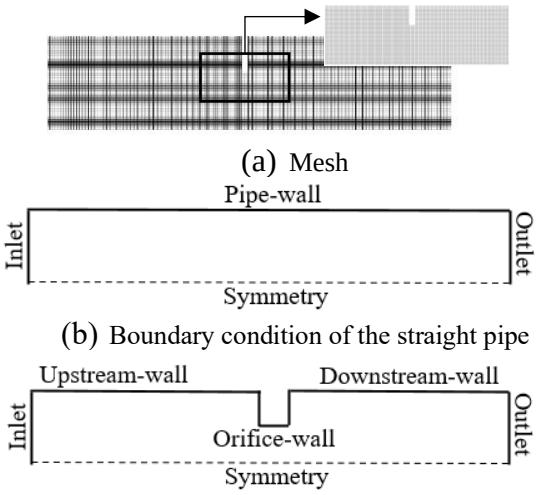

Figure 2. Detail mesh and boundary condition

2.5 Mesh Independence Test

A mesh independence test was performed to minimize discretization errors across different mesh densities. The present study employed three mesh resolutions—coarse (50,000 elements), medium (100,000 elements), and fine (200,000 elements)—by the methodology proposed by Roache [17]. The reference parameter for evaluating mesh sensitivity was the fluid velocity at the coordinate point (x = 0, y = 0). The procedure involved calculating the mesh refinement ratio (Equation 10), determining the order of convergence (Equation 11), and computing the Grid Convergence Index (GCI) between mesh levels using Equations 12 and 13. Specifically, GCI_{fine} was used to assess the error between fine and medium meshes, while GCI_{coarse} evaluated the discrepancy between medium and coarse meshes. The resulting values confirmed that

all mesh variations fell within the convergence range. The lowest numerical error, 1.82%, was observed in the fine mesh, which was subsequently adopted for the main simulations to ensure greater accuracy and convergence.

$$r = \frac{h_2}{h_1} \tag{10}$$

$$\bar{p} = \frac{\ln\left(\frac{f_3 - f_2}{f_2 - f_1}\right)}{\ln(r)} \tag{11}$$

$$GCI_{fine} = \frac{F_s |\varepsilon|}{\left(r^{\bar{p}} - 1\right)} \tag{12}$$

$$GCI_{coarse} = \frac{F_s |\varepsilon| r^{\bar{p}}}{\left(r^{\bar{p}} - 1\right)} \tag{13}$$

$$\varepsilon = \frac{f_{n+1} - f_n}{f_n} \tag{14}$$

$$\frac{GCI_{coarse}}{GCI_{fine} r^{\bar{p}}} \approx 1 \tag{15}$$

$$fr_{h=0} = f_1 + \frac{(f_1 - f_2)}{\left(r^{\bar{p}} - 1\right)} \tag{16}$$

Table 1. Grid independency study result

Mesh	Fine	Medium	Coarse
Velocity	0.18224	0.18252	0.18282
$\bar{p}$		0.11677	
r		2	
GCI_{fine}		2.24%	
GCI_{coarse}		2.43%	
$f_{r_h = 0}$		0.17898	
$\frac{GCI_{fine}}{GCI_{coarse} r^{\bar{p}}}$		1	
Error	**1.82%**	**1.98%**	**2.14%**

3. Result and Discussion

3.1 Validation

The numerical simulation results were checked against the ISO 5167-2 standard values to ensure their accuracy in representing the flow behavior under realistic conditions. The discharge coefficient (C_d) obtained from the simulation was then compared with the ISO 5167-2 standard data at a beta ratio (β) of 0.6 for the Reynolds number range of $10^4 \leq Re \leq 10^6$. As demonstrated in Figure 3, the average error of the discharege coefficient (C_d) values is within the range of ± 2%, and a slight trend difference is observed with the ISO 5167-2 standar data at lower Reynolds number range ($10^4 \leq Re \leq 3.0 \times 10^4$), likely due to numerical instability. At higher Reynolds numbers, the results are consistent with the trend of the ISO 5167-2 standar data. The accuracy tolerance in this study is set at ± 5% of the ISO 5167-2 standard data, to confirms the validity and reliability of the modeling data in subsequent analyses [11].

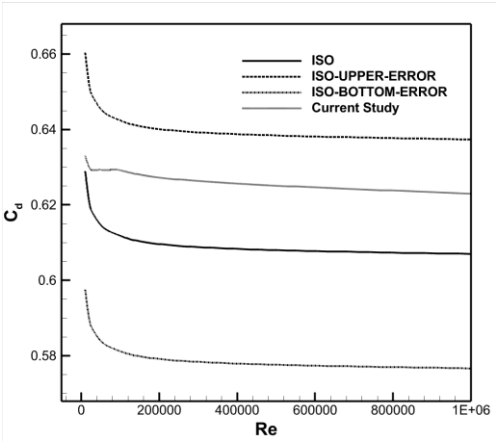

Figure 3. The central limit of the confidence interval for C_d is established at 5% for each specified Reynolds number

3.2 Analysis

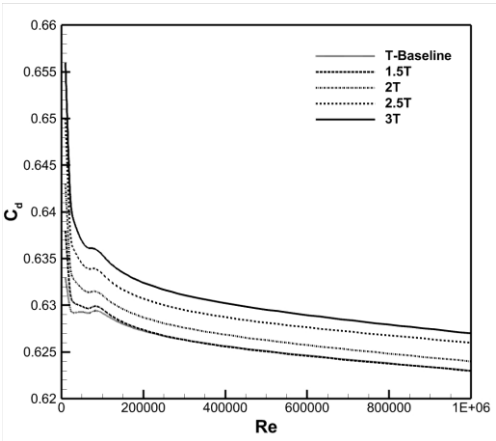

Figure 4. C_d value is determined by orifice plate thickness variation across each Reynolds number

This study considers fluid flow through orifice plates of different

thicknesses at different Reynolds numbers. The flow control efficiency is evaluated using the discharge coefficient (C_d), showing that the C_d of the ISO 5167-2 standard orifice plate (baseline) is lower than that of other orifice plate thickness variations as the Reynolds number increases. The most significant increase is observed in the 3T configuration (Figure 4), consistent with previous studies [18].

The pressure distribution is normalized by the pressure coefficient shown in Figure 5. The C_p value indicates that the pressure is high upstream of the orifice plate and decreases significantly as the fluid passes through the orifice (downstream of the orifice plate), reaching a minimum value of about -2.5 at $x \approx 0.05$ m. After that, the pressure recovers and stabilizes at about $x \approx 0.5$ m. These characteristics are in accordance with the fundamental theory of orifice plates [6, 11]. The pressure drop, which is determined by the difference between the upstream and downstream pressures, reaches a maximum at the base orifice plate, decreases with increasing thickness, and reaches a minimum at 3T. This trend is manifested as an upward shift in the C_p curve. In general, thicker orifices reduce the pressure drop and improve the flow characteristics.

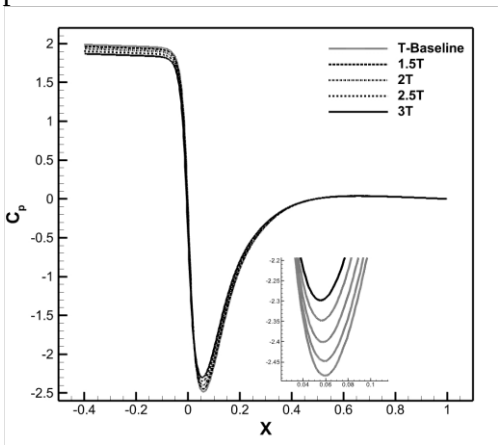

Figure 5. The value of C_p is indicated along the X-axis of the pipe at $Re = 10^4$

The specific pressure drop (ΔP) values are shown in Figure 6 and Table 3. Based on Figure 6, the Reynolds number has a significant effect on ΔP, with higher Reynolds numbers resulting in greater pressure drop. Furthermore, the base orifice plate has the highest ΔP, and ΔP decreases with increasing plate thickness. The lowest pressure drop is observed at 3T, which is approximately 1.35% lower than the base orifice plate with the highest ΔP (Table 3), these results are in line with previous research [18]. Figure 7 illustrates the location of the separation and reattachment points resulting from the interaction between the fluid and the wall (wall shear stress). In the upstream region, the separation point remains similar across various orifice thicknesses due to the uniform pipe geometry. The increasing trend of the C_f curve downstream indicates the formation of a recirculation zone caused by flow separation. As the orifice thickness increases, the recirculation intensity decreases, as evidenced by the shift of the C_f peak toward the negative y-axis. The downstream minimum point on the C_f curve marks the reattachment point (X_r). The baseline orifice plate shows the largest X_r among the others, and a thicker orifice plate results in a shorter reattachment distance, especially at 3T. Additionally, increasing the Reynolds number shifts the reattachment point further downstream, as depicted in Figure 8. The present study illustrates the fluid flow pattern in Figure 9, where a sudden constriction caused by the orifice plate leads to flow separation as the fluid approaches and passes through the orifice. In the downstream region, a recirculation zone forms, producing a vortex structure that results in a reattachment point where the flow re-engages with the surface. The formation of a narrow flow region, known as the vena contracta, is observed as fluid velocity increases through the orifice, characterized by a significant velocity rise, in accordance with the findings in previous research [19].

Figure 10 shows the x-velocity distribution for each orifice plate thickness, where the fluid velocity increases near the orifice to approximately ± 0.12 m/s and reaches a maximum of approximately ± 0.22 m/s at the exit, before gradually decreasing downstream to a steady state. To further

analyze the flow behavior, the velocity profiles at selected axial locations are presented in Figure 11. At a distance of 0.1 m upstream of the orifice, the parabolic velocity profile indicates fully developed flow. Closer to the orifice (0.05 m upstream), the velocity increases due to a sudden narrowing. At the orifice plane (x = 0 m), flow separation is observed, characterized by negative velocities near the wall and an overall increase in velocity. The maximum velocity occurs at a distance of 0.05 m downstream, where the pressure drop near the orifice wall drives the formation of a recirculation zone, as also observed in the streamline and velocity contour plots. Further downstream (0.5 m), the velocity profile returns to a fully developed state. In addition, the orifice plate thickness significantly influences the downstream velocity distribution, especially at a distance of 0.05 m downstream.

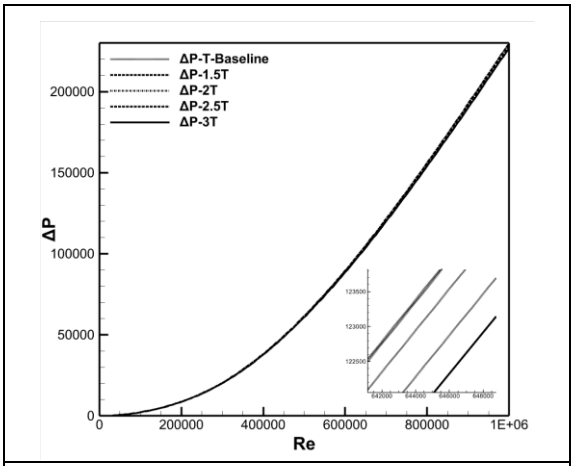

Figure 6. Pressure drop value of orifice plate thickness variation

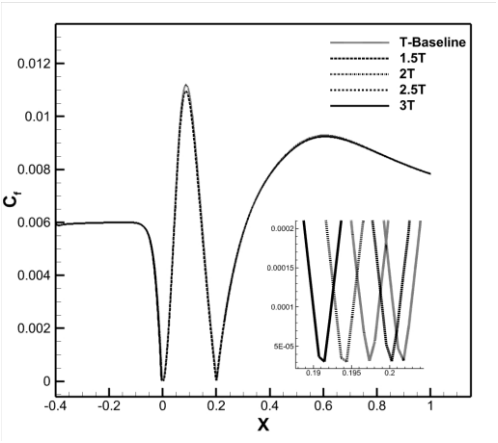

Figure 7. Friction coefficient (C_f) distribution of orifice flow at Re = 10^4

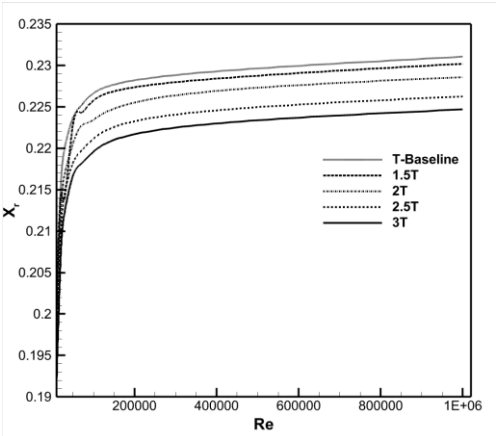

Figure 8. Reattachment point of the orifice plate thickness variation at each Reynolds number

Table 2. Pressure drop value of orifice plate thickness variation at each Reynolds number

Re	ΔP (T)	ΔP (1.5T)	ΔP (2T)	ΔP (2.5T)	ΔP (3T)
10000	22.22784235	21.92820659	21.54616955	21.11355225	20.70367224
20000	89.96144807	89.42889839	88.49282403	87.33719626	86.25819015
30000	202.7278173	202.0061449	200.4286819	198.410804	196.5171445
50000	562.9555982	561.8356552	558.4538762	553.7400539	549.4659303
70000	1103.519606	1101.916685	1096.011881	1087.492336	1079.87516
100000	2252.045831	2249.838797	2238.651206	2222.65302	2208.43613
300000	20458.94817	20463.43867	20375.86119	20253.84684	20149.80945
1000000	229831.9852	229900.0599	229087.0856	227871.6059	226871.1024
Average	31815.54644	31823.80662	31708.31643	31537.02496	31395.27101
Deviation		**0.03%**	**0.34%**	**0.88%**	**1.35%**

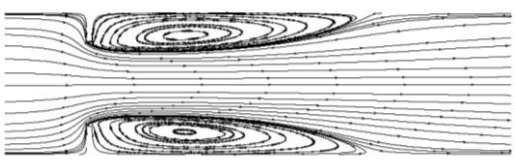

(a) Orifice plate with a thickness of T

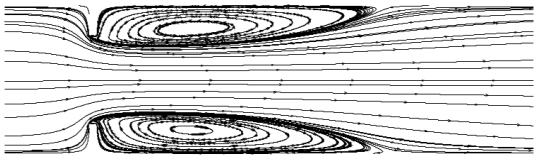

(b) Orifice plate with a thickness of 1.5T

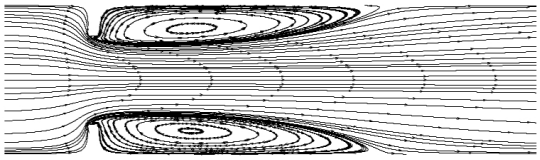

(c) Orifice plate with a thickness of 2T

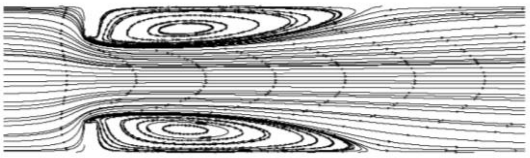

(d) Orifice plate with a thickness of 2.5T

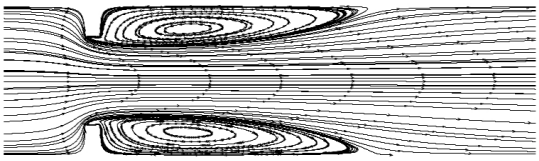

(e) Orifice plate with a thickness of 3T

Figure 9. Streamline contour at Re = 10^4

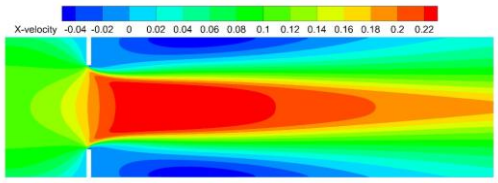

(a) Orifice plate with a thickness of T

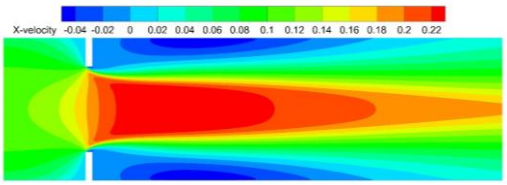

(b) Orifice plate with a thickness of 1.5T

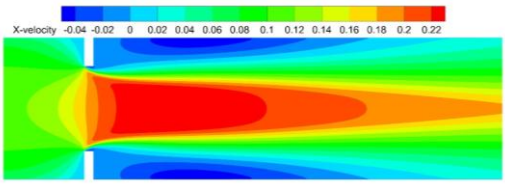

(c) Orifice plate with a thickness of 2T

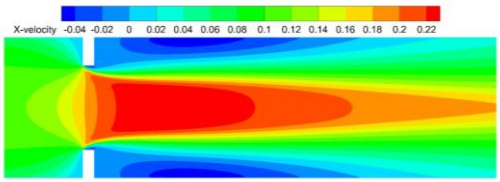

(d) Orifice plate with a thickness of 2.5T

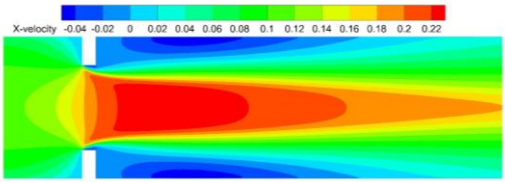

(e) Orifice plate with a thickness of 3T

Figure 10. X-velocity contour at Re = 10^4

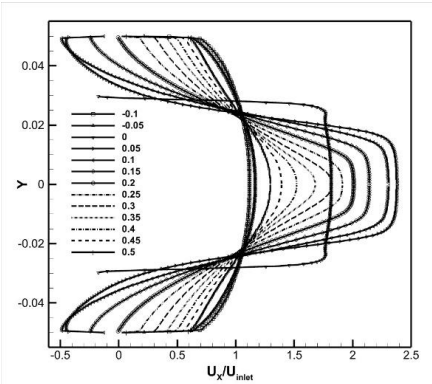

(a) Orifice plate with a thickness of T

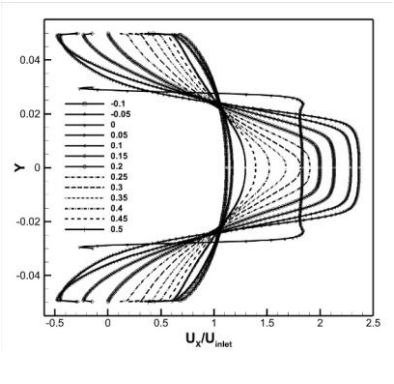

(b) Orifice plate with a thickness of 1.5T

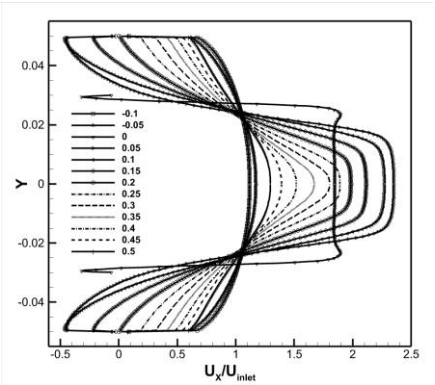

(c) Orifice plate with a thickness of 2T

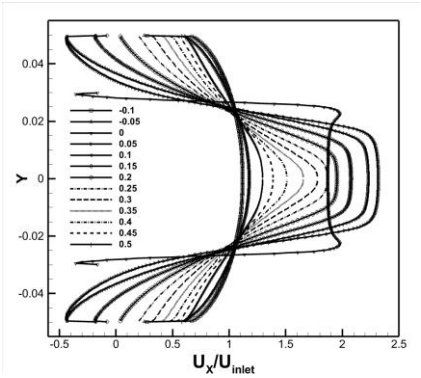

(d) Orifice plate with a thickness of 2.5T

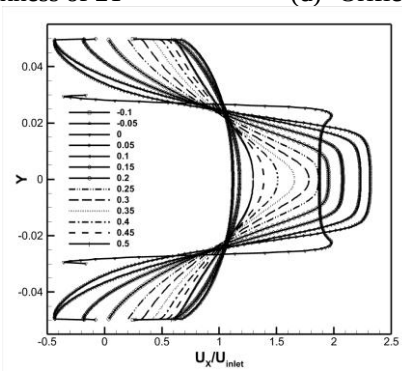

(e) Orifice plate with a thickness of 3T

Figure 11. Velocity profile when passing through the orifice plate at Re = 10^4

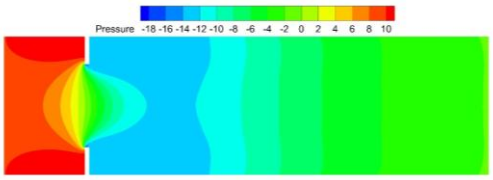

(a) Orifice plate with a thickness of T

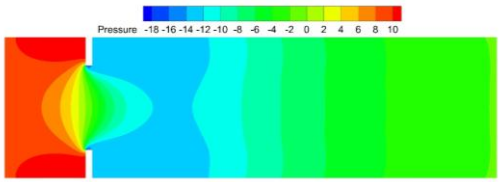

(b) Orifice plate with a thickness of 1.5T

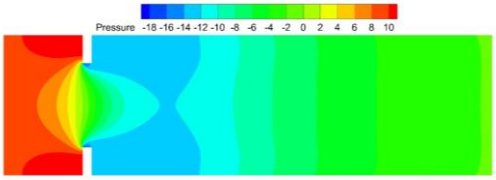

(c) Orifice plate with a thickness of 2T

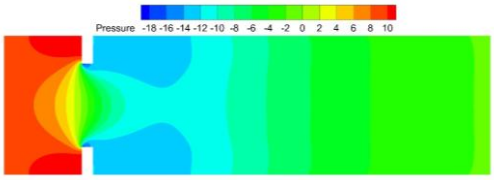

(d) Orifice plate with a thickness of 2.5T

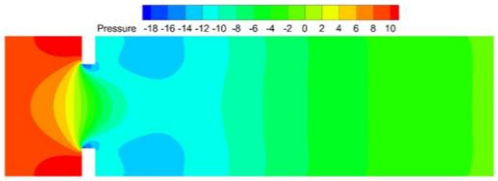

(e) Orifice plate with a thickness of 3T

Figure 12. Pressure contour at Re = 10^4

The relationship between velocity and pressure along the flow path is illustrated in Figure 12. Regions of increasing velocity correspond to a pressure drop from approximately ± 6 Pa to ± −18 Pa, in accordance with Bernoulli's principle and continuity [13]. The pressure and velocity gradients indicate the presence of shear layers, flow separation, and recirculation as the fluid passes through the orifice plate. A significant pressure drop occurs on the downstream side of the orifice plate. Based

on the pressure contours, the 3T orifice plate exhibits a more stable pressure gradient than the thin orifice plate, thus improving downstream flow stability. This indicates that increasing the orifice plate thickness improves pressure distribution, reduces excessive pressure drop, and lowers the risk of cavitation and surface damage. These results are consistent with previous studies [13, 18, 19]. Therefore, optimizing the orifice plate thickness is necessary to minimize pressure-related problems and maintain the structural integrity of the piping system.

4. Conclusion

This study examines the effect of orifice plate thickness on fluid flow characteristics through numerical simulations based on the ISO 5167-2 standard. Conducted within a Reynolds number range of 10^4 to 10^6, the analysis reveals that increasing plate thickness reduces pressure drop and enhances the discharge coefficient, with the 3T plate showing the most improvement (1.35% reduction). Flow separation and recirculation zones near the orifice walls influence skin friction and pressure distribution. Thicker plates also lead to shorter reattachment distances and more stable flow behavior. Overall, the results demonstrate that optimizing orifice thickness improves flow control stability and may reduce mechanical stress within piping systems.

References

[1] S. Kiriella *et al.*, "Effect of internal pressure on the flexural fatigue behaviour of trenchless internal replacement pipe systems," *Tunnelling and Underground Space Technology*, vol. 154, p. 106111, Dec. 2024, doi: 10.1016/j.tust.2024.106111.

[2] C. M. T. Tien *et al.*, "Effects of the legacy pipe ends on the behaviour of pipe-in-pipe repair systems under internal pressure," *Eng Fail Anal*, vol. 144, Feb. 2023, doi: 10.1016/j.engfailanal.2022.106957.

[3] S. P. Hong et al., "Enhanced elastic stress solutions for junctions in various pipe bends under internal pressure and combined loading (90° pipe bend, U-bend, double-bend pipe)," *International Journal of Pressure Vessels and Piping*, vol. 212, Dec. 2024, doi: 10.1016/j.ijpvp.2024.105343.

[4] C. R. Mali et al., "CFD study on the effect of various geometrical parameters of honeycomb type orifices on pressure drop and cavitation characteristics," *Nuclear Engineering and Design*, vol. 370, Dec. 2020, doi: 10.1016/j.nucengdes.2020.110880.

[5] Y. Wu et al., "Experimental study on effect of structural parameters on pressure drop characteristics of multi orifice plates," *Flow Measurement and Instrumentation*, vol. 91, Jun. 2023, doi: 10.1016/j.flowmeasinst.2023.102346.

[6] S. Metering, "FUNDAMENTALS OF ORIFICE METERING."

[7] A. Cioncolini et al., "Micro-orifice single-phase liquid flow: Pressure drop measurements and prediction," *Exp Therm Fluid Sci*, vol. 65, pp. 33–40, Jul. 2015, doi: 10.1016/j.expthermflusci.2015.03.005.

[8] Y. Wu et al., "Experimental study on effect of structural parameters on pressure drop characteristics of multi orifice plates," *Flow Measurement and Instrumentation*, vol. 91, Jun. 2023, doi: 10.1016/j.flowmeasinst.2023.102346.

[9] H. Qin et al., "Experimental and numerical investigation on the hydraulic characteristics of orifice plate throttle for sodium-cooled fast reactor," *Ann Nucl Energy*, vol. 215, Jun. 2025, doi: 10.1016/j.anucene.2025.111269.

[10] S. Nasiruddin and S. N. Singh, "Performance evaluation of an innovative design modification of an orifice meter," *Flow Measurement and Instrumentation*, vol. 80, Aug. 2021, doi: 10.1016/j.flowmeasinst.2021.101944.
[11] "ISO 5167-2 Measurement of fluid flow by means of pressure differential devices inserted in circular-cross section conduits running full-Part 2: Orifice plates," 2003. [Online]. Available: www.iso.org
[12] A. Akhyan and Mhd. Arviansyah, "Pengaruh Variasi Tebal Orifice Lubang Tunggal Terhadap Pressure Drop dan Discharge Coefficient Pada Daerah Entrance dan Fully Developed," *Turbo : Jurnal Program Studi Teknik Mesin*, vol. 12, no. 2, Dec. 2023, doi: 10.24127/trb.v12i2.2235.
[13] M. Okiishi and H. Rothmayer, "Fluid Mechanics." [Online]. Available: www.wileyplus.com
[14] J. Julian et al., "The Influence of Fillet Step on Backward-Facing Step Flow Characteristics," *Infotekmesin*, vol. 14, no. 2, pp. 318–326, Jul. 2023, doi: 10.35970/infotekmesin.v14i2.1919.
[15] N.-S. Kim et al., "Investigation on Fluid Flow Characteristics of the Orifice in Nuclear Power Plant," 2011.
[16] H. Düz, "Effect of conical angle on the hydraulic properties of orifice plate flows: A numerical approach," *Flow Measurement and Instrumentation*, vol. 81, Oct. 2021, doi: 10.1016/j.flowmeasinst.2021.102026.
[17] P. J. Roache, "Perspective: A Method for Uniform Reporting of Grid Refinement Studies," 1994. [Online]. Available: http://fluidsengineering.asmedigitalcollection.asme.org/
[18] B. Gulsacan et al., "Effect of orifice thickness-to-diameter ratio on turbulent orifice flow: An experimental and numerical investigation," 2024, doi: https://doi.org/10.1016/j.icheatmasstransfer.2023.107213.
[19] T. Tunay et al., "Investigation of laminar and turbulent flow through an orifice plate inserted in a pipe," 2004.